International Journal of Pharmaceutics 551 (2018) 322–328

Contents lists available at ScienceDirect

International Journal of Pharmaceutics

journal homepage: www.elsevier.com/locate/ijpharm

Optimized acriflavine-loaded lipid nanocapsules as a safe and effective delivery system to treat breast cancer

Yoann Montigaud[a,b], Bernard Ucakar[a], Balaji Krishnamachary[c], Zaver M. Bhujwalla[c,d], Olivier Feron[e], Véronique Préat[a], Fabienne Danhier[a], Bernard Gallez[b,*], Pierre Danhier[f]

[a] Université catholique de Louvain, Louvain Drug Research Institute, Advanced Drug Delivery and Biomaterials, Avenue Mounier 73, B1.73.12, 1200 Brussels, Belgium
[b] Université catholique de Louvain, Louvain Drug Research Institute, Biomedical Magnetic Resonance Research Group Platform, Avenue Mounier 73, B1.73.08, 1200 Brussels, Belgium
[c] Division of Cancer Imaging Research, In Vivo Cellular and Molecular Imaging Center, The Russell H. Morgan Department of Radiology and Radiological Science, The Johns Hopkins University School of Medicine, Baltimore, MD, USA
[d] Sidney Kimmel Comprehensive Cancer Center, The Johns Hopkins University School of Medicine, Baltimore, MD, USA
[e] Université catholique de Louvain, Pole of Pharmacology and Therapeutics (FATH), Institut de Recherche Expérimentale et Clinique (IREC), Avenue Mounier 53, B1.53.09, 1200 Brussels, Belgium
[f] Université catholique de Louvain, Louvain Drug Research Institute, Nuclear and Electron Spin Technologies (NEST) Platform, Avenue Mounier 73, B1.73.07, 1200 Brussels, Belgium

ARTICLE INFO

Keywords:
Lipid nanocapsules
Drug delivery system
Breast cancer
Acriflavine
4T1 cells
Design of experiments (DoE)

ABSTRACT

Acriflavine (ACF) hydrochloride is currently repurposed as multimodal drug, inhibiting hypoxia-inducible factors (HIF) pathways and exerting cytotoxic properties. The aim of this study was to encapsulate ACF in reverse micelles and to incorporate this suspension in lipid nanocapsules (LNC). Designs of experiments were used to work under quality by design conditions. LNC were formulated using a phase-inversion temperature method, leading to an encapsulation efficiency around 80%. *In vitro*, the encapsulated drug presented similar cytotoxic activity and decrease in HIF activity in 4T1 cells compared to the free drug. *In vivo*, ACF-loaded nanoparticles (ACF dose of 5 mg/kg) demonstrated a higher antitumor efficacy compared to free ACF on an orthotopic model of murine breast cancer (4T1 cells). Moreover, the use of LNC allowed to drastically decrease the number of administrations compared to the free drug (2 *versus* 12 injections), suppressing the ACF-induced toxicity.

1. Introduction

Among all cancers, breast cancer (BC) is the most encountered one in women, no matter how developed countries are. In 2012, worldwide incidence was about 1.7 million cases. That represents 25.2% of total cancers in women, making BC the most spread among women, behind lung cancer. Moreover, it is the deadliest cancer among women with a mortality of 14.7% (Bray et al., 2008; Ferlay et al., 2012; Torre et al., 2016). It reached 6.2 million cases in 2012, representing 36.6% of women cancer and 19.2% of worldwide cancer (Ferlay et al., 2012). Currently, first treatment of BC is surgical resection of the tumor, associated or not with radiotherapy of chest wall, axillar and parasternal lymph nodes to avoid metastasis. When tumors are not operable, chemotherapies and radiotherapies are associated. When BC becomes metastatic, only palliative cares are available. Main sites of metastasis are lungs, brain and bones (Gilkes and Semenza, 2013). Systemic treatments include endocrine or chemotherapies, bisphosphonates and targeted biological agents such as trastuzumab (Cardoso et al., 2012).

Acriflavine (ACF) is an old topical anti-protozoal and anti-bacterial antibiotic. ACF is known to sensitize to radiotherapy, to inhibit epithelial-to-mesenchymal transition, to activate p53 leading to cell death and to induce mitochondrial or endoplasmic reticulum apoptosis and autophagy (Shay et al., 2014; Lee et al., 2009; Lim et al., 2012). This molecule is mainly used in preclinical antitumor studies to inhibit hypoxia-inducible factors (HIF) (Lee et al., 2009). HIF is a heterodimer transcription factor composed of an α and β subunit. Under normoxia, HIF-1α is continuously degraded due to the presence of an oxygen-dependent degradation (ODD) domain. Indeed, HIF-1α is hydroxylated, enabling its binding to von Hippel-Lindau protein, which induces its proteasomal degradation. Under hypoxia, HIF-1α is stabilized and binds to its β subunit in the nucleus. This heterodimer then binds to hypoxia-response elements (HRE) in promoter regions of genes that allow adaptation to hypoxic stress (Shay et al., 2014). Physiologically, this mechanism allows cells to survive under mild hypoxia such as

* Corresponding author.
E-mail address: bernard.gallez@uclouvain.be (B. Gallez).

https://doi.org/10.1016/j.ijpharm.2018.09.034
Received 29 June 2018; Received in revised form 3 September 2018; Accepted 15 September 2018
Available online 17 September 2018
0378-5173/

physical activity. In cancer, the vasculature is anarchic, which leads to chronic hypoxia (Liu et al., 2015). As a consequence, HIF-related genes are a key player in cancer by promoting survival, proliferation and metastasis (Semenza et al., 1996; Nguyen et al., 2009; Wong et al., 2011, 2012). In BC, these genes induce the formation of niches that lead to lung metastasis, which are related to high aggressiveness and mortality (Shay et al., 2014; Liu et al., 2015). Since ACF directly blocks HIF dimerization (Lee et al., 2009), there is a rationale to improve the therapeutic arsenal to block tumor progression due to HIF overexpression. In BC, HIF is related to poor prognosis due to chemoresistance, invasiveness and metastasis (Gilkes and Semenza, 2013). Hence, developing therapeutics targeting HIFs could be a promising strategy to improve BC treatments. However, ACF shows a very low biological half-life of 7 min in rats and exerts a toxicity leading to a loss of body weight (Kim et al., 1997).

Consequently, we hypothesized that the use of a drug delivery system could overcome these limitations. However, for most of nanocarriers, synthesis processes (*i*) require to use organic solvents, (*ii*) are time consuming and (*iii*) need costly devices such as high-pressure homogenizer or rotavapor. Accordingly, we decided to use lipid nanocapsules (LNC) as carriers. These particles are formulated using the phase-inversion temperature method (Heurtault et al., 2002; Anton et al., 2008; Anton and Vandamme, 2009; Vrignaud et al., 2011). This is a low-energy and free solvent method using components generally recognized as safe (GRAS) according to health authorities. Few years ago, Vrignaud et al. (2012) successfully encapsulated hydrophilic drugs in reverse micelle-loaded LNC.

In this study, we hypothesized that encapsulation of ACF into LNC could be useful to repurpose the use of ACF to treat cancer by protecting the drug from degradation, reduce its toxicity and improve the delivery into tumors. Then, we will first optimize this carrier and encapsulate ACF by design of experiments (DoE) to obtain good encapsulation efficiency. Second, we will assess the anti-HIF activity of ACF-loaded LNCs *in vitro* in murine BC cells. Thirdly, antitumor activity of ACF (free *versus* encapsulated) in a murine orthotopic BC model.

2. Materials and methods

2.1. Materials

Oil solubilizers were a gift from Gattefossé S.A (Saint-Priest, France). ACF powder, Span® 80 (sorbitan monooleate), Tween® 80 (polyoxyethylenesorbitan monooleate) and Kolliphor® HS 15 (mixture of free polyethylene glycol 660 and polyethylene glycol 660 hydroxystearate) were purchased from Sigma-Adlrich (Overijse, Belgium). Lipoid® S 75 (soybean lecithin at 70% of phopshatidylcholine) was a gift from Lipoid Gmbh -Ludwigshafen, Germany). Sodium chloride was purchased from Prolabo VWR International (Fontenay-Sous-Bois, France). Purified water was obtained from a MilliQ System (Millipore, Paris, France). Liquid chromatography solvents were purchased from Sigma-Aldrich (Overijse, Belgium). DMEM™ (41965-039), DMEM™Glutamax (61965-026), PBS pH 7.4 (10010-023), FBS (10500-064), Sodium Pyruvate (11360-039), L-Glutamine (25030-24) and 0.05%Trypsin-EDTA (25300-054) were purchased from Thermo Fisher Scientific (Asse, Belgium). Puromycin 100 mg/mL was purchased from InvivoGen (San Diego, USA). TransIT®-2020 Transfection Reagent was purchased from Mirus Bio (Madison, USA).

2.2. Quantification of drugs

Quantification of ACF was performed with a HPLC system (Shimadzu Prominence HPLC, Japan) composed of a LC-20AT separation module coupled with a SIL-20A HT autosampler. A SPD-20A UV/visible detector and a CT0-20A oven. Analytical separations were performed on Xbridge® C18 grafted phenyl column (4.6 × 150 mm; 3 µm). HPLC analyses were carried out at 50 °C with a mobile phase of TFA 0.05%/methanol (30/70) at flow rate of 0.8 mL/min. Absorbance wavelength was set at 262 nm. Linearity was obtained from 0 to 100 µg/mL with a LOD of 0.784 µg/mL and a LOQ of 2.38 µg/mL.

2.3. Incorporation of ACF in reverse micelles

Solubilization of ACF in reverse micelles was tested by adding 75 µL of ACF solution at 1 mg/ml in 600 mg of reverse micelles. After centrifugation (15 000*g*, 5 min, 4 °C) reverse micelles precipitated and formed a gel. Supernatant was removed and precipitated reverse micelles were disrupted by adding methanol with a ratio over 1:40. ACF content in supernatant and reverse micelles were quantified by HPLC as previously described. To determine which couples of surfactant and oils could be used for solubilizing ACF, two experiments were performed. First, screening of surfactant and oil was realized to determine which surfactant/oil couples could form reverse micelles. Second, design of experiments (DoE) was realized with selected surfactant/oil couples. Parameters of DoE were: ratio of surfactant/oil; type of surfactant; type of oil (Anton et al., 2010).

2.4. Formulation of reverse micelles-loaded lipid nanocapsules

Reverse micelles were prepared by stirring surfactant and oil, at a ratio of 1/5, and then adding 75 µL solution of ACF at 100 mg/mL. LNC were prepared using a modified phase-inversion temperature (PIT) method (Heurtault et al., 2002). Briefly, Kolliphor® HS15 (39.3%), sodium chloride (1.8%), oil (17.2%) and water (41.7%) were mixed by magnetic stirring at 750 rpm. When used, Lipoid® S75 is used at 1.5%. Four heating-cooling cycles from 45 °C to 90 °C were applied. During last cycle, when temperature reached 85 °C, 500 µL of preheated ACF-loaded reverse micelles were added to the mixture. Then, system was cooled to reach the PIT and 2.5 mL of icy water was added and stirred for one minute.

To optimize the formulation of reverse micelles-loaded LNC, a DoE was performed. Tested factors were surfactant/oil couples and the impact of Lipoid® on formulation. Surfactant/oil couples with more interesting response were selected. We performed a second DoE to study the impact of Lipoid® S75 and surfactant/oil couples with the highest encapsulation efficiency. At least 1/3 of experiments were assessed another time to be used as test points. Then, impact of the volume of ACF solution was studied to determine the most suitable parameter.

DoEs were conceived and statistically treated with NemrodW® software (NemrodW, Marseille, France). Studied responses were size, polydispersity index (PDI), zeta (ζ) potential, encapsulation efficiency. In each DoE, each condition was triplicated.

2.5. Physico-chemical characterization of LNC

2.5.1. Particle size and ζ potential measurements

Size distribution was determined by dynamic light scattering and ζ potential was measured by electrophoretic light scattering in MilliQ water using Zetasizer® Nano ZS series (Malvern Instruments, Worcestershire, UK). Measurements were performed with a 633 nm helium-neon laser, 4 mW, at 25 °C in backscattering mode (reading angle 173°). PDI, which represents broadness of size distribution (ISO 13321:1996), was calculated from mean size x and standard deviation σ of Gaussian distribution obtained from cumulant analysis using Eq. (1). Each measurement was carried out in triplicates.

$$PDI = \frac{x}{\sigma} \quad (1)$$

2.5.2. Encapsulation efficiency

Total amount of drug was determined by breaking nanoparticles in methanol with a dilution factor of 1/40. Free and encapsulated drug were separated by ultrafiltration using Amicon® centrifuge filters

(MWCO: 30 kDa, 4000g, 4 °C, 20 min). Filtrates were diluted with a dilution factor of 1/4. Samples were quantified by HPLC a previously described. Encapsulation efficiency (EE) was calculated by using Eq. (2).

$$EE(\%) = \frac{encapsulatedamountofdrug}{totalamountofdrug} \times 100\% \quad (2)$$

2.5.3. Stability and release in dispersion medium

One milliliter of ACF-loaded LNC were placed in a dialysis bag Float-a-Lyzer® G2 with a MWCO of 50 kDa (Spectrum Labs, Overijse, Belgium), put in 20 mL PBS pH 7.4. System was kept at 37 °C under magnetic stirring at 300 rpm. Until 72 h, 1 mL of dispersion medium was withdrawn and replaced with 1 mL of preheated fresh medium to maintain sink conditions. At the end of experiment, nanoparticles were removed and size, PDI and EE were assessed.

2.6. In vitro experiments

2.6.1. Cell culture

4T1 murine BC cells were kindly provided by Dr. Fred Miller (Karmanos Cancer Institute). During experiments, cells were used from P1 to P20. 4T1 cells were incubated at 37 °C in humidified atmosphere under 5% CO_2 in DMEM™ Glutamax supplemented with 10% FBS.

2.6.2. Transfection of HRE-ODD-LUC plasmid in 4T1 cells for HIF activity measurements

4T1 cells were seeded in 6-well plates at 30–40% cell density. After 24 h, cells were transfected with a plasmid encoding the luciferase gene fused to ODD under the control of a poly-HRE sequence (5xHRE) using TransIT®-2020 Transfection Reagent (Danhier et al., 2015; Stable Cell Line, 2017; Harada et al., 2007). Cells were grown in puromycin-containing medium (3 µg/ml) and a clone was isolated (Stable Cell Line, 2017).

2.6.3. Bioluminescence and viability assay

Twenty thousand 4T1-HRE-ODD-luc cells were seeded in 24-well plates cells for 24 h. Then, media were replaced with fresh media containing control or treatments. Cells were incubated under 21% or 1% O_2 (5% CO_2) to mimic normoxia and hypoxia (Ruskin, INVIVO$_2$® 400). After 24 h of incubation, media were replaced by 400 µL of luciferin in PBS at 150 µg/ml (Saha et al., 2011). Bioluminescence imaging (BLI) was performed with Xenogen IVIS™ 50 (Perkin Elmer, Walthm, USA). Exposure time was set at 2 min. Quantification was realized with Living Image® 3.2 software. As each plate had a positive control (maximum signal in wells without treatments), results are expressed as relative intensity, thus allowing comparison between different plates from different experiments. To assess cell viability at the end of experiment, PBS was replaced by a solution of crystal violet (0.23%) for 30 min. Crystal violet was removed, wells were rinsed with clear water and allowed to dry overnight.

2.7. In vivo antitumor efficacy of ACF

All experiments were performed in compliance with guidelines set by national regulations and were approved by the ethical committee for animal care of the health sciences sector of the Université catholique de Louvain.

Tumors were measured with an electronic calliper and tumor volume was characterized using the following formula (3):

$$Tumor\ volume = \frac{lenght \times width^2 \times \pi}{6} \quad (3)$$

2.7.1. In vivo antitumor efficacy of free ACF

4T1 cells (2.10^5 cells per mouse) were injected in the mammary fat pad in the right flank of BALB/cAnNRJ (female, 7 weeks old), purchased from Janvier Labs (Le Genest-Saint-Isle, France). Treatments started 4 days after tumor induction. Two groups were defined: group 1 – PBS (n = 6) and group 2 – ACF 5 mg/kg (n = 6). ACF and PBS were daily administered by intraperitoneal injections. Tumor volume and weight of mice were measured every two days. Endpoints were set at 400 mm^3 of tumor volume or 20% of body weight loss.

2.7.2. In vivo antitumor efficacy of ACF-loaded LNC

4T1 cells (2.10^5 cells per mouse) were injected in the mammary fat pad in the right flank of BALB/cAnNRJ (female, 7 weeks old), purchased from Janvier Labs (Le Genest-Saint-Isle, France). Treatments started 4 days after tumor induction. Four groups were defined: group 1: PBS (n = 8), group 2: ACF 5 mg/kg (n = 6), group 3: LNC of ACF 5 mg/kg (n = 5) and group 4: Unloaded LNC (n = 6). ACF and PBS were daily administered by intraperitoneal injections. LNC were weekly injected by intravenous injection in the tail vein. Tumor volume and weight of mice were assessed every two days. Endpoints were set at 400 mm^3 of tumor volume or 20% of body weight loss.

2.8. Statistical analyses

Statistical analyses were performed using GraphPad Prism® 7 for Windows®. *In vitro* experiments were expressed as mean ± SD and analysed using one-way ANOVA with Tukey's multiple comparison test. *In vivo* experiments were expressed as mean ± SEM and analysed using two-way ANOVA, multiple comparison tests were performed with Tukey or Sidak adjustments.

3. Results and discussion

3.1. In vivo antitumor efficacy of free ACF

To determine which concentration of ACF could be effective on an orthotopic mouse model of BC, we performed an anti-tumor efficacy study. Fig. 1 A, B shows that daily administration of ACF at 5 mg/kg significantly delayed tumor growth ($p < 0.001$). The antitumor efficacy of ACF at 2 mg/kg was lower than those of ACF at 5 mg/kg (daily administration) ($p < 0.033$ and $p < 0.002$, respectively) (data not shown). However, ACF 5 mg/kg exerts a toxicity (weight loss), as shown in Fig. 1C. Therefore, we will use LNC to encapsulate ACF at the dose of 5 mg/kg aiming at decrease its toxicity while maintaining its antitumor efficacy.

3.2. Development and optimization of ACF-loaded LNC using designs of experiments (DoE)

Once we determined the dose of ACF to incorporate in LNC (5 mg/kg), we focused on the development of the nanocarrier aiming at obtaining good encapsulation efficiency.

3.2.1. Incorporation of ACF in reverse micelles

The solubilisation step is a critical step in low-energy nano-emulsification process. ACF is a strongly hydrophilic drug. As we intended to encapsulate into a lipidic core of LNC, we needed to develop a double emulsion process. Hence, ACF was solubilised in reverse micelles of Span® 80 or Tween® 80 in different oils (Supplementary data 1). Tested surfactants were Span® and Tween® 80 due to their biocompatibility (Strickley, 2004; Rowe et al., 2009; Prieto and Calvo, 2013) and their previous use in reverse micelles loaded-LNC (Vrignaud et al., 2011, 2012). As incorporation of the drug highly impacts encapsulation efficiency of nanoparticles, we optimized the encapsulation efficiency of ACF in reverse micelles. We used DoE to determine which suitable surfactant/oil couples showed the highest encapsulation efficiency. Factors of this DoE were type of surfactant, surfactant/oil ratio and type of oil. Following this DoE, three surfactant/oil couples were selected:

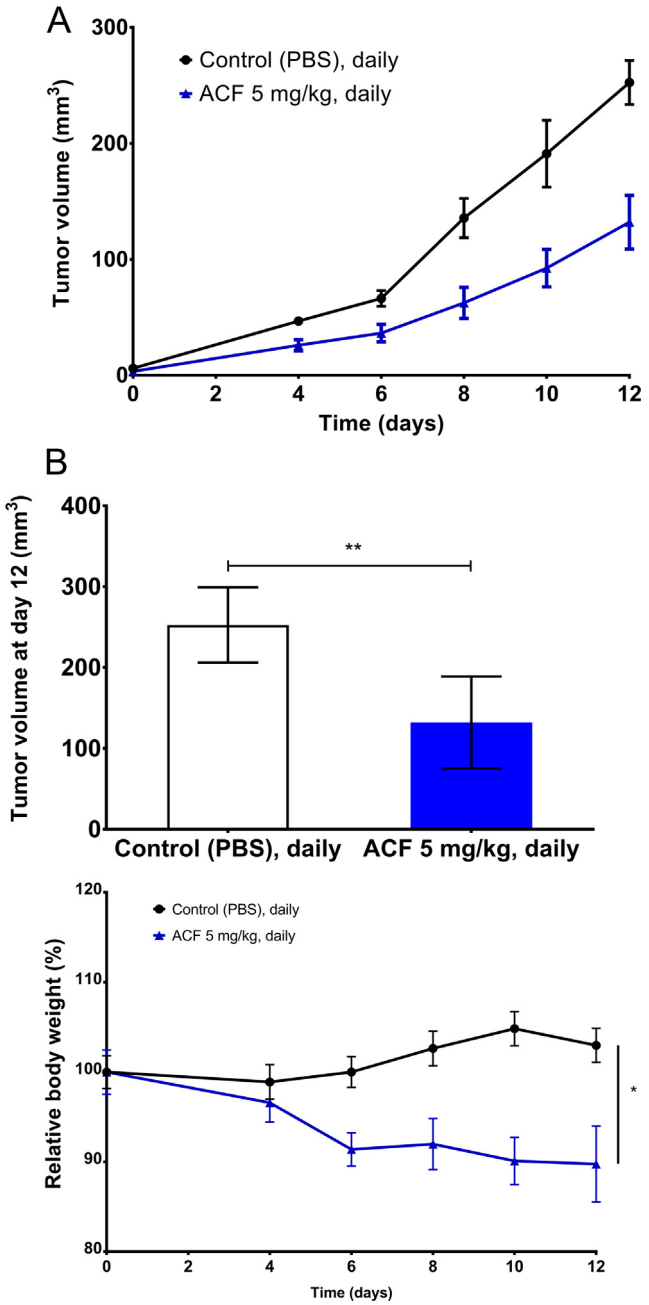

Fig. 1. Antitumor efficacy of free ACF. (A) Tumor volume in mm^3 *versus* time in 4T1 tumor-bearing mice. (B) Bar plot of tumor volume for each group at day 12 of the experiment. (C) Relative body weight of mice *versus* time. Data are shown as mean ± SD. In all panels, * and ** correspond to $p < 0.05$ and < 0.01.

Tween® 80/ Labrafil® M 2125, Tween® 80/ Labrafac® PG and Span® 80/Labrafac® WL 1349. We decided to use Tween® 80 because it allows decreasing the amount of surfactant. Span® 80/Labrafac® WL 1349 has been tested because it is the historical couple of surfactant and oil and therefore used as reference (Vrignaud et al., 2012).

3.2.2. Formulation of reverse micelles-loaded LNC

Selected surfactant/oil couples listed above are used as factors in another DoE to assess which one leads to the highest encapsulation efficiency in LNC. The other factor is the presence or absence of Lipoid® S75 in the mixture. Indeed, this component is usually used during development of LNC and increases stability of the carrier due to its ability to solidify at 4 °C, creating a rigid shell at the interface (Heurtault et al., 2002, 2003). Studied responses are size and encapsulation efficiency. PDI of all formulations is always under 0.1, showing the strongly monodisperse nature of formulations (Supplementary data 2). These results are in accordance with those obtained from previous DoE on reverse micelles. LNC synthesized with Tween® 80/Labrafil® M 2125 and Span® 80/Labrafac® WL 1349 were stable over a week at 4 °C in terms of size, PDI and encapsulation efficiency.

Table 1 shows characteristics of LNC prepared during DoE. As shown, there is no difference in term of size and PDI between formulations with and without Lipoid®. Main changes are on encapsulation efficiency and ζ potential. Higher encapsulation efficiency could be due to increase stability of LNC avoiding leakage during cooling dilution. Lower zeta potential is due to choline moiety of Lipoid® S 75 that increased recruitment of negative charges at the surface of nanoparticle. Therefore, Lipoid® was included in LNC as it has a significant impact on encapsulation efficiency and it increases stability of LNC (Heurtault et al., 2003; Vonarbourg et al., 2005).

To assess effect of the volume of ACF used to load reverse micelles, three different volumes were tested in triplicate. Table 2 shows results of this experiment. Lower volumes increased encapsulation efficiency without modifying size, PDI nor ζ potential. Obviously, decreasing volume of ACF decreased drug loading. Thus, we decided to set the volume of ACF at 50 µL, which is a compromise between lowering the carrier amount and obtaining a good yield of ACF incorporation.

3.2.3. Stability and release study in dispersion medium

Fig. 2 shows percentage of cumulative release of ACF from ACF-loaded LNC in PBS *versus* time. The release phase (80% release of ACF) occurred within the first 8–10 h After 72 h of release, only 26.2% ± 2.8% of total ACF was recovered: 23.9% ± 2.5% in LNC and 2.3% ± 0.3% free. This suggests that encapsulation could prolong the short half-life of ACF (10 min) (Song et al., 2005).

3.3. In vitro studies: HIF inhibition by free and encapsulated ACF

To assess if ACF-loaded LNC could inhibit HIF activity, 4T1 cells were transfected with a plasmid encoding the luciferase gene, fused to ODD, under the promotion of a poly-HRE sequence. Under hypoxia and

Table 1
Size, PDI, Zeta potential and encapsulation efficiency of LNC obtained with the design of experiments (DoE). Data are expressed as mean ± SD.

0% of Lipoid®				
Surfactant/oil couples	Size (nm)	PDI	Zeta potential (mV)	EE (%)
Tween® 80/Labrafil® M 2125	32.14 ± 3.22	0.049 ± 0.022	0.24 ± 0.82	64.30 ± 3.37
Tween® 80/Labrafac® PG	48.32 ± 2.19	0.037 ± 0.004	0.54 ± 0.032	54.93 ± 2.22
Span® 80/Labrafac® WL 1349	52.91 ± 1.81	0.047 ± 0.015	0.43 ± 0.19	55.59 ± 2.16
1.5% of Lipoid®				
Surfactant/oil couples	Size (nm)	PDI	Zeta potential (mV)	EE (%)
Tween® 80/Labrafil® M 2125	30.98 ± 4.69	0.037 ± 0.004	-2.66 ± 1.93	66.14 ± 4.02
Tween® 80/Labrafac® PG	45.05 ± 6.32	0.046 ± 0.021	-2.02 ± 0.43	61.10 ± 1.79
Span® 80/Labrafac® WL 1349	49.79 ± 3.96	0.054 ± 0.011	-6.48 ± 5.84	58.39 ± 5.31

Table 2
Impact of volume of ACF on the characteristics of LNC. Data are expressed as mean ± SD.

Volume of ACF	Size (nm)	PDI	Zeta potential (mV)	EE (%)
75 µL	30.98 ± 4.69	0.037 ± 0.004	−2.66 ± 1.93	66.14 ± 4.02
50 µL	29.21 ± 1.24	0.033 ± 0.004	−2.52 ± 1.20	82.87 ± 1.84
25 µL	29.35 ± 0.30	0.038 ± 0.003	−3.31 ± 1.79	87.42 ± 0.20

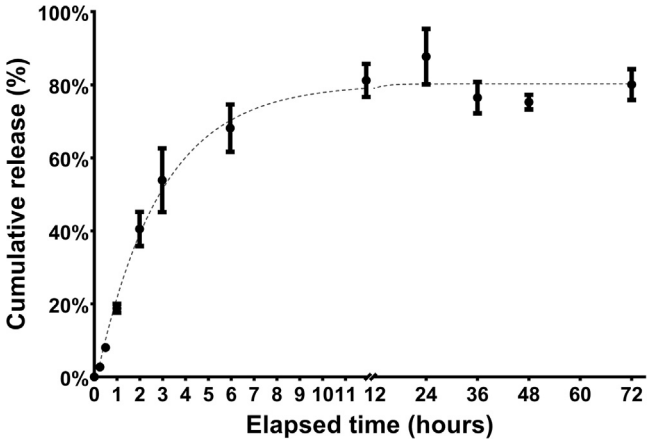

Fig. 2. Release profile of ACF-loaded LNC in PBS for 3 days (n = 3). Results are expressed in mean ± SD. Dotted line represents fitting of the release.

in the presence of luciferin, a bioluminescence signal can be measured, which correlates to HIF activity (Harada et al., 2007; Danhier et al., 2015). 4T1 cells were incubated during 24 h with free or encapsulated ACF at increasing concentrations, under hypoxic or normoxic conditions. Fig. 3A shows an important decrease in BLI signal even for low ACF concentrations. No difference was found between free and encapsulated ACF concentration. These data clearly demonstrated that ACF does not lose its activity when encapsulated.

To determine if the inhibition of BLI signal was due to HIF inhibition or cell death, we realized a cell viability assay using crystal violet staining. Fig. 3B demonstrates a dose-dependent loss of cell viability with encapsulated ACF. Briefly, crystal violet staining showed that free ACF did not exert any effect on cell proliferation, whereas ACF-loaded LNC had a limited cytotoxic effect on 4T1 cells. This increased cytotoxicity could be explained by a different mechanism of cell uptake of LNC compared to free drug. While most of drugs enter into cells by passive diffusion or via specific transporters, LNC are described to be taken up by endocytosis. Hence, at higher concentrations, transporters could be saturated while the endocytosis remains efficient (Bastiancich et al., 2016; Garcion et al., 2006; Paillard et al., 2010). As previously described, blank LNC did not show any cytotoxicity (Bastiancich et al., 2016). At 0.375 µM ACF-loaded LNC, we observed a strong inhibition of HIF activity and no sign of cytotoxicity. These results confirmed that encapsulated ACF block HIF activity similarly to the free drug.

3.4. Antitumor efficacy of free and encapsulated ACF

The *in vivo* anti-tumor efficacy of ACF-loaded LNC compared to free ACF, blank LNC and PBS was evaluated on an orthotopic murine model of BC (4T1). We tested ACF at the dose of 5 mg/kg since previous experiments showed anti-tumor efficacy but presented some toxicity (body weight loss) when the drug was not encapsulated in LNC. All treatments induced a delay in tumor growth when compared to control group (Fig. 4). Groups treated with ACF-loaded LNC showed a significant difference compared with blank LNC-, free ACF- and PBS-treated groups. As expected, blank LNC group showed similar tumor growth curves than PBS. This observation evidenced that unloaded-nanoparticles are nontoxic. Interestingly, free ACF at 5 mg/kg (daily injections) showed important signs of toxicity (body weight loss),

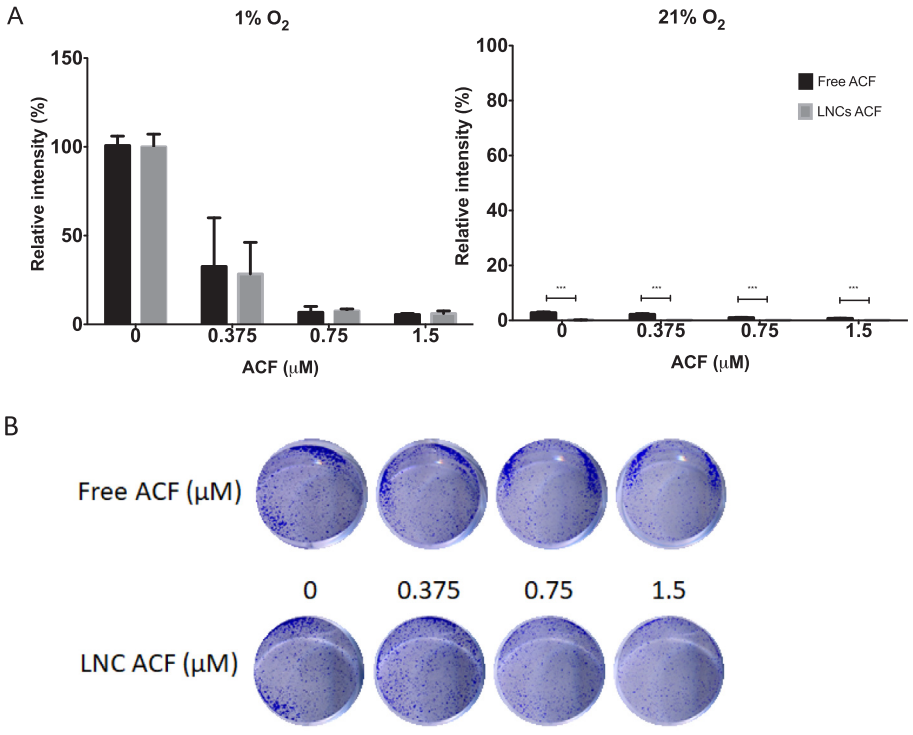

Fig. 3. (A) Relative intensity of BLI signal induced by HIF activation *versus* increasing concentrations of ACF in hypoxia and normoxia. Data are presented in mean ± SD. (B) Pictures of bioluminescent signal and cytotoxicity assed by crystal violet *versus* increasing concentrations of ACF in hypoxic conditions. *** correspond to $p < 0.001$.

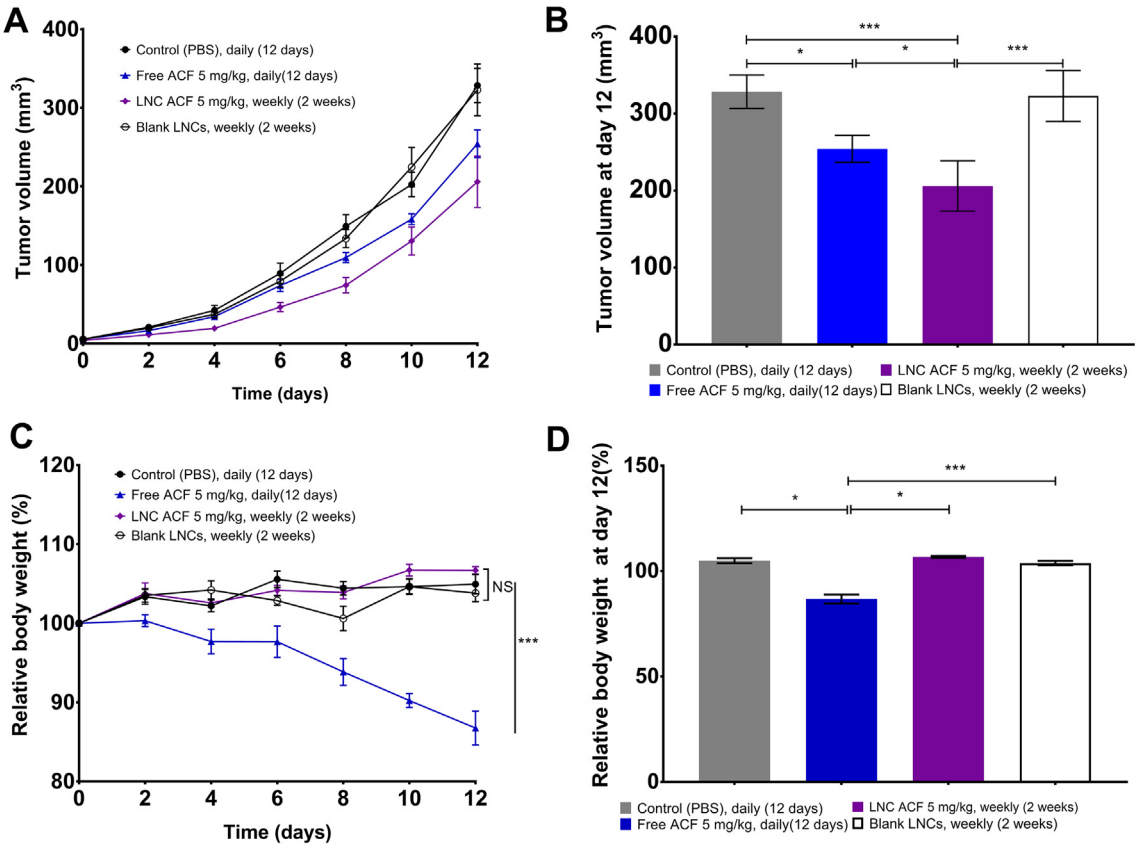

Fig. 4. Compared *in vivo* antitumor efficacy of free ACF and ACF-loaded LNC on orthotopic 4T1 tumor-bearing mice. (A) Evolution of tumor growth *versus* time. (B) Histogram plotting tumor volume at day 12 after treatment initiation. (C) Relative body weight variations *versus* time. (D) Histogram plotting relative body weight at day 12 after treatment initiation. Data are shown as mean ± SEM. *, ** and *** correspond to $p < 0.05$, 0.01 and 0.001.

whereas mice treated with ACF-loaded LNC at 5 mg/kg (weekly injections) had a similar body weight compared to the control groups. A higher antitumor effect was obtained with encapsulated ACF compared to free ACF ($p < 0.05$). It is crucial to note that free drug was daily administered (12 injections), whereas ACF-loaded LNC were administered once a week during 2 weeks. In other words, ACF-loaded LNCs (total injected dose of 2 × 5 mg/kg) were more efficacious to treat 4T1 tumor bearing mice and less toxic compared to daily injections of free ACF (total injected dose of 60 mg/kg). This observation could be due to (i) the putative enhanced half-life time of ACF obtained with the encapsulation in LNC (Song et al., 2005), (ii) the enhanced permeability and retention (EPR) effect, which could contribute participates to the increased antitumor effect of ACF-loaded LNCs compared to free ACF. Altogether, these results highlight the usefulness of LNC. Indeed, when ACF is encapsulated in LNC, we obtained a higher antitumor efficacy with (*i*) a decreased frequency of administration (once per week during 2 weeks *versus* a daily administration for 12 consecutive days) and (*ii*) a lower toxicity.

4. Conclusions and perspectives

In this study, we developed new nanomedicine containing a promising HIF inhibitor (ACF) for cancer therapy. The aim of this study was to develop a nanocarrier able to satisfactory encapsulate ACF, an hydrophilic drug, which presents two problems to be overcome: (i) a very short biological half-life and (ii) an *in vivo* toxicity on 4T1-tumor bearing mice or on other tumor-bearing mice (Song et al., 2005), at concentrations of ACF of 5 mg/kg with daily intraperitoneal injections.

We successfully encapsulated ACF in reverse micelle-loaded LNC. Further DoE experiments allowed to optimize the nanomedicine formulation, aiming at improving the biological half-life and decreasing ACF toxicity *in vivo* through a decrease of ACF administrated doses. ACF-loaded LNC showed a size around 30 nm, a strong monomodal dispersion and an encapsulation efficiency over 80%. The release profile of ACF-loaded LNC occurred with a burst release of 12 h followed by a sustained release of ACF for at least 8 h. Of note, the encapsulated ACF release will be faster in biological media such as serum. We showed however that the use of LNCs to encapsulate ACF warrants an increase in the antitumor activity and a decrease in the toxicity *in vivo*. *In vitro*, we determined cell viability of ACF-loaded LNC and HIF activity inhibition in 4T1-HRE-ODD-luc cells after exposure of free and encapsulated ACF under hypoxic conditions. Although we observed some cytotoxic effect due to the presence of LNC, we determined that encapsulated drug exerted a similar decrease in HIF activity compared to the free drug at low dose (0.375 µM). Importantly, no cytotoxicity was observed at 0.375 µM ACF in both groups. *In vivo*, we observed a higher antitumor efficacy of ACF-loaded LNC (ACF dose of 5 mg/kg) compared to free ACF. Moreover, the use of LNC allowed (*i*) to drastically decrease the number of administrations compared to the free drug (2 *versus* 12 injections) and (*ii*) to suppress the ACF-induced toxicity.

In vitro and *in vivo* assays could be performed to determine sensitivity of other tumor cell lines with different HIF expression status to ACF and to characterize the potential benefit of encapsulated ACF on tumor growth *in vivo*. Indeed, other tumor models have been treated with ACF, regarding the literature, mainly epithelial or glandular tumors (Shay et al., 2014; Lee et al., 2009). An interesting perspective would be to correlate tumor response and HIF activity in these tumor types. Lastly, some therapies are known to increase HIF-1α signalization pathways, leading to resistance to treatments or resurgence, such as doxorubicin or photodynamic therapy (Lee et al., 2014; Hassan et al., 2011; Fan et al., 2014; Weijer et al., 2015; Cao et al., 2013, 2016; Dekervel et al., 2016; Peltonen et al., 2010; Cuyàs et al., 2015). Hence,

the use of ACF-loaded LNC in combination with these therapies could overcome these side effects.

Acknowledgments

This study was supported by the Belgian National Fund for Scientific Research – Fonds National de la Recherche Scientifique (F.R.S.- FNRS) and the Fondation contre le cancer (Belgium). The authors have no conflicts of interest to declare.

Appendix A. Supplementary data

Supplementary data to this article can be found online at https://doi.org/10.1016/j.ijpharm.2018.09.034.

References

Anton, N., Mojzisova, H., Porcher, E., Benoit, J.-P., Saulnier, P., 2010. Reverse micelle-loaded lipid nano-emulsions: new technology for nano-encapsulation of hydrophilic materials. Int. J. Pharm. 398, 204–209.
Anton, N., Vandamme, T.F., 2009. The universality of low-energy nano-emulsification. Int. J. Pharm. 377, 142–147.
Anton, N., Benoit, J.-P., Saulnier, P., 2008. Design and production of nanoparticles formulated from nano-emulsion templates—a review. J. Control. Rel. 128, 185–199.
Bastiancich, C., Vanvarenberg, K., Ucakar, B., Pitorre, M., Bastiat, G., Lagarce, F., Préat, V., Danhier, F., 2016. Lauroyl-gemcitabine-loaded lipid nanocapsule hydrogel for the treatment of glioblastoma. J. Control. Rel. 225, 283–293.
Bray, F., Ren, J.-S., Masuyer, E., Ferlay, J., 2013. Global estimates of cancer prevalence for 27 sites in the adult population in 2008. Int. J. Cancer 132, 1133–1145.
Cao, Y., Eble, J.M., Moon, E., Yuan, H., Weitzel, D.H., Landon, C.D., 2013. Tumor cells upregulate normoxic HIF-1α in response to doxorubicin. Cancer Res. 73, 6230–6242.
Cao, J., Lin, G., Gong, Y., Pan, P., Ma, Y., Huang, P., 2016. DNA-PKcs, a novel functional target of acriflavine, mediates acriflavine's p53-dependent synergistic anti-tumor efficiency with melphalan. Cancer Lett. 383, 115–124.
Cardoso, F., Harbeck, N., Fallowfield, L., Kyriakides, S., Senkus, E., 2012. Locally recurrent or metastatic breast cancer: ESMO Clinical Practice Guidelines for diagnosis, treatment and follow-up. Ann. Oncol. 23, 11–19.
Cuyàs, E., Martin-Castillo, B., Corominas-Faja, B., Massaguer, A., Bosch-Barrera, J., Menendez, J.A., 2015. Anti-protozoal and anti-bacterial antibiotics that inhibit protein synthesis kill cancer subtypes enriched for stem cell-like properties. Cell Cycle 14, 3527–3532.
Danhier, P., Krishnamachary, B., Bharti, S., Kakkad, S., Mironchik, Y., Bhujwalla, Z.M., 2015. Combining optical reporter proteins with different half-lives to detect temporal evolution of hypoxia and reoxygenation in tumors. Neoplasia 17, 871–881.
Dekervel, J., Bulle, A., Windmolders, P., Lambrechts, D., Van Cutsem, E., Verslype, C., 2016. Acriflavine inhibits acquired drug resistance by blocking the epithelial-to-mesenchymal transition and the unfolded protein response. Transl. Oncol. 10, 59–69.
Fan, J., Yang, X., Bi, Z., 2014. Acriflavine suppresses the growth of human osteosarcoma cells through apoptosis and autophagy. Tumor Biol. 35, 9571–9576.
Ferlay, J., Soerjomataram, I., Dikshit, R., Eser, S., Mathers, C., Rebelo, M., 2015. Cancer incidence and mortality worldwide: Sources, methods and major patterns in GLOBOCAN 2012. Int. J. Cancer 136, E359–E386.
Garcion, E., Lamprecht, A., Heurtault, B., Paillard, A., Aubert-Pouessel, A., Denizot, B., Menei, P., Benoît, J.-P., 2006. A new generation of anticancer, drug-loaded, colloidal vectors reverses multidrug resistance in glioma and reduces tumor progression in rats. Mol. Cancer Ther. 5, 1710–1722.
Gilkes, D.M., Semenza, G.L., 2013. Role of hypoxia-inducible factors in breast cancer metastasis. Future Oncol. 9, 1623–1636.
Harada, H., Kizaka-Kondoh, S., Itasaka, S., Shibuya, K., Morinibu, A., Shinomiya, K., Hiraoka, M., 2007. The combination of hypoxia-response enhancers and an oxygen-dependent proteolytic motif enables real-time imaging of absolute HIF-1 activity in tumor xenografts. Biochem. Biophys. Res. Commun. 360 (4), 791–796.
Hassan, S., Laryea, D., Mahteme, H., Felth, J., Fryknäs, M., Fayad, W., 2011. Novel activity of acriflavine against colorectal cancer tumor cells. Cancer Sci. 102, 2206–2213.
Heurtault, B., Saulnier, P., Pech, B., Proust, J.E., Benoît, J.P., 2002. Properties of polyethylene glycol 660 12-hydroxy stearate at a triglyceride/water interface. Int. J. Pharm. 242, 167–170.
Heurtault, B., Saulnier, P., Pech, B., Proust, J.-E., Benoit, J.-P., 2003. Physico-chemical stability of colloidal lipid particles. Biomaterials 23, 4283–4300.
Kim, S.G., Kim, C.W., Ahn, E.T., Lee, K.-Y., Hong, E.-K., Yoo, B.-I., 1997. Enhanced antitumour effects of acriflavine in combination with guanosine in mice. J. Pharm. Pharmacol. 49, 216–222.
Lee, C.-J., Yue, C.-H., Lin, Y.-J., Lin, Y.-Y., Kao, S.-H., Liu, J.-Y., 2014. Antitumor activity of acriflavine in lung adenocarcinoma cell line A549. Anticancer Res. 34, 6467–6472.
Lee, K., Zhang, H., Qian, D.Z., Rey, S., Liu, J.O., Semenza, G.L., 2009. Acriflavine inhibits HIF-1 dimerization, tumor growth, and vascularization. PNAS 106, 17910–17915.
Lim, M.-J., Ahn, J.-Y., Han, Y., Yu, C., Kim, M.-H., Lee, S., 2012. Acriflavine enhances radiosensitivity of colon cancer cells through endoplasmic reticulum stress-mediated apoptosis. Int. J. Biochem. Cell Biol. 44, 1214–1222.
Liu, Z., Semenza, G.L., Zhang, H., 2015. Hypoxia-inducible factor 1 and breast cancer metastasis. J. Zhejiang Univ. Sci. B 16, 32–43.
Nguyen, D.X., Bos, P.D., Massagué, J., 2009. Metastasis: from dissemination to organ-specific colonization. Nat. Rev. Cancer 9, 274–284.
Paillard, A., Hindré, F., Vignes-Colombeix, C., Benoit, J.-P., Garcion, E., 2010. The importance of endo-lysosomal escape with lipid nanocapsules for drug subcellular bioavailability. Biomaterials 31, 7542–7554.
Peltonen, K., Colis, L., Liu, H., Jäämaa, S., Moore, H.M., Enbäck, J., 2010. Identification of novel p53 pathway activating small-molecule compounds reveals unexpected similarities with known therapeutic agents. PLoS One 5.
Prieto, C., Calvo, L., 2013. Performance of the biocompatible surfactant tween 80, for the formation of microemulsions suitable for new pharmaceutical processing. J. Appl. Chem., e930356.
Rowe, R.C., Sheskey, P.J., Quinn, M.E., American Pharmacists Association (Eds.), 2009. Handbook of pharmaceutical excipients, sixth ed. Pharmaceutical Press ; American Pharmacists Association, London ; Chicago : Washington, DC, pp. 888.
Saha, D., Dunn, H., Zhou, H., Harada, H., Hiraoka, M., Mason, R.P., 2011. In vivo bioluminescence imaging of tumor hypoxia dynamics of breast cancer brain metastasis in a mouse model. J. Vis. Exp. 56.
Semenza, G.L., Jiang, B.-H., Leung, S.W., Passantino, R., Concordet, J.-P., Maire, P., 1996. Hypoxia response elements in the aldolase A, enolase 1, and lactate dehydrogenase A gene promoters contain essential binding sites for hypoxia-inducible factor 1. J. Biol. Chem. 271, 32529–32537.
Shay, J.E.S., Imtiyaz, H.Z., Sivanand, S., Durham, A.C., Skuli, N., Hsu, S., 2014. Inhibition of hypoxia-inducible factors limits tumor progression in a mouse model of colorectal cancer. Carcinogenesis 35, 1067–1077.
Song, S., Kwon, O.S., Chung, Y.B., 2005. Pharmacokinetics and metabolism of acriflavine in rats following intravenous or intramuscular administration of AG60, a mixture of acriflavine and guanosine, a potential antitumour agent. Xenobiotica 35, 755–773.
Stable Cell Line Generation|Mirus Bio LLC [Internet]. [Cited 2017 Jun 9]. Available from: https://www.mirusbio.com/applications/stable-cell-line-generation.
Strickley, R.G., 2004. Solubilizing excipients in oral and injectable formulations. Pharm. Res. 21, 201–230.
Torre, L.A., Siegel, R.L., Ward, E.M., Jemal, A., 2016. Global cancer incidence and mortality rates and trends—an update. Cancer Epidemiol. Biomarkers Prev. 25, 16–27.
Vonarbourg, A., Saulnier, P., Passirani, C., Benoit, J.-P., 2005. Electrokinetic properties of noncharged lipid nanocapsules: Influence of the dipolar distribution at the interface. Electrophoresis 11, 2066–2075.
Vrignaud, S., Anton, N., Gayet, P., Benoit, J.-P., Saulnier, P., 2011. Reverse micelle-loaded lipid nanocarriers: a novel drug delivery system for the sustained release of doxorubicin hydrochloride. Eur. J. Pharm. Biopharm. 79, 197–204.
Vrignaud, S., Hureaux, J., Wack, S., Benoit, J.-P., Saulnier, P., 2012. Design, optimization and in vitro evaluation of reverse micelle-loaded lipid nanocarriers containing erlotinib hydrochloride. Int. J. Pharm. 436, 194–200.
Weijer, R., Broekgaarden, M., Krekorian, M., Alles, L.K., van Wijk, A.C., Mackaaij, C., 2015. Inhibition of hypoxia inducible factor 1 and topoisomerase with acriflavine sensitizes perihilar cholangiocarcinomas to photodynamic therapy. Oncotarget 27, 3341–3356.
Wong, C.C.-L., Gilkes, D.M., Zhang, H., Chen, J., Wei, H., Chaturvedi, P., 2011. Hypoxia-inducible factor 1 is a master regulator of breast cancer metastatic niche formation. PNAS 108, 16369–16374.
Wong, C.C.-L., Zhang, H., Gilkes, D.M., Chen, J., Wei, H., Chaturvedi, P., 2012. Inhibitors of hypoxia-inducible factor 1 block breast cancer metastatic niche formation and lung metastasis. J. Mol. Med. 90, 803–815.